

On the Eddy Isopycnal Thickness Diffusivity of the Gent-McWilliams Subgrid Mixing Parameterization

Mototaka Nakamura and Yi Chao
Jet Propulsion Laboratory
California Institute of Technology

June 10, 1999

Abstract

Output of an eddy-resolving model of the North Atlantic Ocean is used to diagnose the eddy thickness diffusivity coefficient, κ , defined by Gent and McWilliams (1990) in their quasi-adiabatic parameterization for transports by mesoscale eddies. The results suggest that κ has large spatial and temporal variations, with negative values about half of the time. The order of magnitude of κ shows a wide range in the western North Atlantic, varying from $10m^2s^{-1}$ to $10^7m^2s^{-1}$. Also, the value of κ is considerably affected by the time scale used to define the high-frequency and low-frequency components. The results suggest that κ should be a diagnosed variable that reflects the strength of eddy mixing during a model integration.

*mixing
parameterization*

1 Introduction

Parameterizing effects of mesoscale eddies on large-scale fields of density, tracers, and momentum in coarse-resolution ocean models has been an important and difficult task. With the present computing power, it is not feasible to integrate eddy-resolving ocean models in a wide parameter space until the deep oceans reach a statistical equilibrium, not to mention eddy-resolving models coupled to atmospheric general circulation models. Investigations of climatic phenomena that require consideration of deep oceans will inevitably depend on coarse-resolution ocean models for some time to come. The importance of heat and salt transports by oceans in maintenance of and fluctuations in the global and regional climates has become increasingly clear, necessitating realistic parametric representations of heat and salt transports by the most energetic part of the oceanic currents associated with mesoscale eddies in coarse-resolution ocean models.

A major improvement in representation of density and tracer mixing by eddies in coarse-resolution ocean models was proposed by Gent and McWilliams (1990) (GM90, hereafter) and has been implemented and examined in various contexts, ranging from a 2-dimensional model with an initialized front (Gent et al., 1995, GM95 hereafter) to a primitive equation ocean GCM with thermohaline and wind forcings (Danabasoglu et al., 1994). The improvement over the conventional isotropic horizontal diffusion that has been widely used is based on a theory that eddies mix isopycnal layer thickness along isopycnal surfaces in such a way that they redistribute water mass within an isopycnal layer adiabatically. GM90 proposed an advective representation of effects of eddies by deriving a formulation for the "eddy-induced transport velocity" from the theory of adiabatic mixing of isopycnal layer thickness. By replacing the horizontal diffusion parameterization of tracers with the advective plus isopycnal diffusion parameterization proposed by GM90, Danabasoglu et al. (1994) demonstrated that a substantial warming of the thermocline that occurs in models with ordinary

diffusion parameterization can be significantly reduced by the GM90 parameterization. A major reason for the overall improvement in temperature and salinity simulation by the GM90 parameterization is that the representation of eddy fluxes by the eddy-induced transport velocity mimics the fact that divergence of the fluxes due to large-scale flows and eddies tend to cancel out. Although the overall simulation results for temperature and salinity were improved, the new parameterization made temperature too cold and salinity too fresh at deep levels, below 2000m or so, in their experiments. Several recent studies report the beneficial effect of the GM90 parameterization in 3-dimensional primitive equation ocean general circulation models (OGCM), while they also find the excessive cooling and freshening of deep water (Duffy et al., 1995a, 1995b; Robitaille and Weaver, 1995; Duffy et al., 1997).

In the GM90 parameterization, two major parameters are left for specification in an OGCM. One is the isopycnal thickness diffusivity coefficient, κ , and the other is the isopycnal stirring coefficient, μ . Although constant positive values have been used for these coefficients in the past studies (Danabasoglu et al., 1994; Duffy et al., 1995a, 1995b; Robitaille and Weaver, 1995; Duffy et al., 1997), these coefficients may well have spatial and temporal variations and may be even locally negative, as suggested by GM90. The GM90 parameterization is designed to mimic the qualitative effect of eddies on large-scale density structures on a basin scale, i.e., baroclinic eddies are expected to be a negative definite sink of large-scale potential energy when an entire basin is considered (GM95). However, specification of κ and μ based on the structure of the large-scale oceanic state may improve the parameterization further. Maps of sea surface height variability and eddy kinetic energy indicate that these coefficients that represent the mixing strength of eddies may have a great spatial variation (Stammer et al., 1996).

The idea of specifying a variable κ based on the structure of the large-scale flows was proposed and tested in a study by Visbeck et al. (1997). Based on theories of

baroclinic eddy mixing by Green (1970) and Stone (1972), Visbeck et al. suggest specification of κ related to the growth rate of the most unstable baroclinic wave in the Eady model (Eady, 1949) of baroclinic instability and the width of the baroclinic zone. The specification of κ in this manner is also supported by a scaling argument by Held and Larichev (1996) and a good structural agreement between the observed sea surface height variance and the growth rate computed from the Levitus (1982) climatology (Treguier et al., 1997). However, the lack of observational data has prohibited a direct estimation of κ for the real oceans. Here, we attempt to estimate values of κ in the vicinity of the Gulf Stream (GS), using output of an eddy-resolving model of the North Atlantic basin as pseudo-data. As noted by GM90 and GM95, κ and μ are not necessarily the same and may well be determined by different factors. We focus on κ in the present work due to the difficulty in estimating μ with our model output. Section 2 briefly describes the model output used for the diagnoses, while section 3 describes the formulation of the GM90 parameterization and a method of diagnoses. Results of the diagnoses are described and discussed in section 4.

2 Pseudo-data

The pseudo-data used for the calculations are from a 30-year integration of a primitive-equation, free-surface eddy-resolving GCM of the North Atlantic described by Chao et al. (1996). The model basin covers the Atlantic basin from 35°S to 80°N and from 100°W to 20°E. The horizontal grid spacing of the model is approximately 1/6° (0.1875° in longitude and 0.1843° in latitude). There are unevenly spaced 37 vertical levels in the model. Near the artificial closed boundaries of the model ocean, temperature and salinity are restored toward seasonal climatology of Levitus (1994). The portion of integration from which we extract the output is driven with the surface salinity restored toward the Levitus climatology (Levitus, 1994), the surface heat flux derived from the European Center for Medium-Range Weather Forecast (ECMWF) analysis, and the surface wind stress derived from the ECMWF analysis. The model

performance on the GS system is described in Chao et al. (1996). The model has reproduced some of the observed characteristics of the GS reasonably well, including the separation point and the mean path of the GS. The model GS does, however, show unrealistic features. In particular, the model GS has significantly stronger quasi-stationary meanders along its path downstream of the separation point than does the observed. Also, the model GS underestimates kinetic energy considerably compared to some observational values at depth (Owens, 1991; Richardson, 1993). Also, farther downstream, the characteristic 90° northward turn of the current toward the North-western Corner is not well-reproduced in the model. Rather than turning northward, the current becomes split, producing some flow turning north and some flow shooting toward northeast. This problem has been observed in other North Atlantic Ocean simulations by eddy-permitting and eddy-resolving OGCMs (e.g., Bryan and Holland, 1989; Semtner and Chervin, 1992; Smith et al., 1992; Beckmann et al., 1994).

We focus our attention on the domain covering 30°N - 60°N and 75°W - 15°W for the present work. The choice is made to cover most of the GS after separation from the western boundary and the North Atlantic Current, as well as quieter parts the North Atlantic away from these currents. The 3-dimensional model output is available at every grid point every 3 days. This sampling frequency is sufficient to obtain smooth evolution of temperature and salinity fields, as well as the velocity field, from the archived output. The portion of the model output employed for the diagnostics is from March of Year 25 to February of Year 30. During this 5-year period, 600 snapshots of potential temperature, salinity, and horizontal velocity are available.

3 Formulation of the GM scheme and diagnostic procedure

GM90 suggest parameterizing effects of mesoscale eddies on large-scale density and tracer structures in a form of adiabatic redistribution of water mass within a layer

bounded by two isopycnal surfaces. It is accomplished by mixing of isopycnal layer thickness along isopycnal surfaces and advecting tracers by the eddy-induced transport velocity derived from the isopycnal thickness mixing. The proposed formulation of the eddy-induced transport velocity is designed to mimic the tendency of eddy density flux divergence to cancel out the mean density flux divergence (GM90). The formulation of the eddy-induced transport velocity, \mathbf{V}^* , is as follows:

$$\mathbf{V}_{\mathbf{h}}^* = \frac{\partial}{\partial z} \left(\kappa \frac{\nabla_{\mathbf{h}} \bar{\sigma}}{\bar{\sigma}_z} \right) \quad (1)$$

and

$$w^* = -\nabla_{\mathbf{h}} \cdot \left(\kappa \frac{\nabla_{\mathbf{h}} \bar{\sigma}}{\bar{\sigma}_z} \right). \quad (2)$$

Here, σ is potential density and κ is the eddy isopycnal thickness diffusivity coefficient to be specified in models. An overbar and a subscript \mathbf{h} denote, respectively, the low-frequency component and the horizontal component of a vector. A subscript z denotes the direction of differentiation. As pointed out by Visbeck et al. (1997), this formulation is essentially the residual mean velocity that forms the transformed Eulerian mean velocity, $\overline{\mathbf{V}_{\mathbf{T}}}$, defined by Andrews and McIntyre (1979) as follows:

$$\overline{\mathbf{V}_{\mathbf{hT}}} = \overline{\mathbf{V}_{\mathbf{h}}} + \mathbf{V}_{\mathbf{h}}^* \quad (3)$$

and

$$\overline{w_{\mathbf{T}}} = \overline{w} + w^*, \quad (4)$$

where a subscript \mathbf{T} denotes the total advective velocity. With this representation of the total transport velocity, $\overline{\mathbf{V}_{\mathbf{T}}}$, GM90 and GM95 suggest use of the following equation for time integrations of tracers in coarse-resolution ocean models:

$$\frac{\partial \bar{\chi}}{\partial t} + \overline{\mathbf{V}_{\mathbf{T}}} \cdot \nabla \bar{\chi} = \bar{s} + D_i(\bar{\chi}). \quad (5)$$

Here, χ is any tracer, s represents source/sink of χ , and $D_i(\bar{\chi})$ is the isopycnal diffusion term represented by a rotated diffusion tensor (Solomon, 1971; Redi, 1982). As noted in GM90, $D_i(\bar{\sigma}) = 0$ by definition and, thus, in the interior, where $\bar{s} \approx 0$, the following holds:

$$\frac{\partial \bar{\sigma}}{\partial t} + \overline{\mathbf{V}_T} \cdot \nabla \bar{\sigma} = 0. \quad (6)$$

As mentioned in the introduction, the above representation of eddy transport has been used and found to improve an overall simulation of large-scale oceanic states and tracer distributions by coarse-resolution OGCMs, while it has also been found to make deep waters too cold and too fresh (Danabasoglu et al., 1994; Duffy et al., 1995a, 1995b; Robitaille and Weaver, 1995; Duffy et al., 1997). A question remains as to whether the scheme represents the reality and, if it does, appropriate values of κ . Rix and Willebrand (1996) attempted to evaluate the GM scheme, using output of an eddy-permitting model, and found that their diagnoses support the validity of the GM scheme, although their results were obtained from a limited area, in which eddy activity is weak, after considerable averaging of the output. They estimated the mean value of κ in their domain of calculation to be on the order of $1000 m^2 s^{-1}$. Their results, shown in their Fig 1, suggest that κ may have considerable spatial variations, including some locally negative values, even in the relatively quiet domain considered by them. Although the GM90 parameterization is usually implemented with a constant value for κ , eddy activity is known to have great spatial and temporal variations (e.g., Schmitz, 1996; Stammer et al., 1996) and, thus, specification of a variable κ that reflects such variations in eddy activity is more desirable. Using a scaling argument, Held and Larichev (1996) suggest that the eddy mixing strength is proportional to the growth rate of baroclinic waves in the Eady problem (Eady, 1949). Also, Visbeck et al. (1997) suggest specification of κ based on ideas proposed by Green (1970) and Stone (1972) and propose a formulation that incorporates the growth rate of baroclinic waves in the Eady problem (Eady, 1949). The κ diagnosed from the

Levitus (1982) data set, using their formulation, suggests locally large eddy activity in the vicinity of the GS, Kuroshio, and Antarctic Circumpolar Currents (Treguier et al. [1997]; Nakamura and Marshall, unpublished calculations), consistent with the observed sea surface height variance and eddy kinetic energy (e.g, Stammer et al., 1996). There has been no confirmation, however, that such horizontal distribution is appropriate for κ .

To obtain an approximate 3-dimensional field of κ from the pseudo-data, we use a diagnostic formula derived from the definition of the eddy-induced velocity and the low-frequency density equation as described in the following. We first note that the tendency equation for $\bar{\sigma}$ with the GM parameterization yields, ideally,

$$\nabla \cdot \overline{\mathbf{V}'\sigma'} = \nabla \cdot (\mathbf{V}^*\bar{\sigma}), \quad (7)$$

where a prime denotes a high-frequency or eddy component of a variable, e.g., $\sigma' = \sigma - \bar{\sigma}$. Then, from Eqs 1, 2, and 7, we have

$$\bar{\sigma}_z \frac{\partial}{\partial x} \left(\kappa \frac{\bar{\sigma}_x}{\bar{\sigma}_z} \right) + \bar{\sigma}_z \frac{\partial}{\partial y} \left(\kappa \frac{\bar{\sigma}_y}{\bar{\sigma}_z} \right) - \bar{\sigma}_x \frac{\partial}{\partial z} \left(\kappa \frac{\bar{\sigma}_x}{\bar{\sigma}_z} \right) - \bar{\sigma}_y \frac{\partial}{\partial z} \left(\kappa \frac{\bar{\sigma}_y}{\bar{\sigma}_z} \right) = -\nabla \cdot \overline{\mathbf{V}'\sigma'}, \quad (8)$$

where subscripts x , y , and z denote directions of derivatives. Ideally, the above equation should be solved numerically for κ , since all other variables are known. However, such solutions require a sophisticated numerical technique and are beyond the scope of the current work. Here, we use an approximate formula to obtain an estimate for κ . By assuming that spatial variations in κ is much smaller than those in low-frequency isopycnal slopes, we obtain an approximate expression for κ from Eq 8;

$$\kappa \approx \frac{-\nabla \cdot \overline{\mathbf{V}'\sigma'}}{\bar{\sigma}_z \frac{\partial}{\partial x} \left(\frac{\bar{\sigma}_x}{\bar{\sigma}_z} \right) + \bar{\sigma}_z \frac{\partial}{\partial y} \left(\frac{\bar{\sigma}_y}{\bar{\sigma}_z} \right) - \bar{\sigma}_x \frac{\partial}{\partial z} \left(\frac{\bar{\sigma}_x}{\bar{\sigma}_z} \right) - \bar{\sigma}_y \frac{\partial}{\partial z} \left(\frac{\bar{\sigma}_y}{\bar{\sigma}_z} \right)}. \quad (9)$$

We emphasize that the assumption of much smaller variations in κ with respect to isopycnal slopes may not be justified well. However, for the purpose of obtaining an

estimate for κ in the current work, we use Eq 9 and note the uncertainty associated with the approximation.

We computed κ for each time frame of the model output, using a time frequency filter used by Lau and Lau (1984) to separate the total field into the low- and high-frequency parts, and applying Eq 9 to the filtered time series. In practice, we compute the low-frequency component and define the rest as the high-frequency eddy in order to ensure zero overlapping between the low- and high-frequency parts and to retain all fluxes. Note that computation of the low-frequency part of eddy correlation terms, such as $\overline{u'\sigma'}$, requires filtering of the time series twice. We performed two sets of calculations of κ using Eq 9; in one set, we used 150 days for the filter frequency cut-off, while we used 360 days in the other. For the 150-day filter, we used a 151-point time filter, i.e., we used 453 days to compute the low- and high-frequency components at one time frame. For the 360-day filter, due to the limitation in the number of time frames available, we used a 265-point time filter, i.e., we used 795 days to compute the filtered quantities at one time frame. Thus, we have obtained time series of κ for 300 and 72 time frames (or 900 and 216 days), respectively, from calculations with a 150-day filter and a 360-day filter. Low-pass filtered density field shows some slow eddy motions when the frequency cut-off is 150 days, but does not show any vigorous mixing associated with rapid growth, breaking, and decay of mesoscale eddies. Low-frequency density field filtered by a 360-day filter shows very little evolution, not to mention the lack of eddy motions. By calculating κ with different frequency cut-offs, we examine the sensitivity of our results to the choice of the frequency cut-off used to define the low- and high-frequency components. We do not claim either one is better than the other here and will simply mention some differences found in the results of the two sets of calculations. GM95 suggests that the low-frequency filter should be applied both in time and space. We used a large-scale state obtained from averaging the output in time and space ($2^\circ \times 2^\circ$ grids) to check the sensitivity of the results to spatial averaging. We also repeated the calculations with the model's subgrid

diffusive flux divergence included in $\nabla \cdot \overline{\mathbf{V}'\sigma'}$ to examine sensitivity of the results to the unresolved part of the eddy fluxes in the model. The divergence of the subgrid diffusive fluxes is calculated in a manner that is consistent with the diffusive scheme used in the model integration.

4 Results and discussions

Fig 1 shows a typical horizontal structure of κ in the top 400m at one time frame, calculated with the frequency cut-off of 150 days. The most striking feature in this figure is negative values in roughly half of the area considered here. There is no visible systematic relationship between the areas of negative values and the low-frequency flow field and the areas of negative values change noticeably in time. The same is true for κ calculated with a 360-day filter also. At all model levels and all time frames, roughly half of the values are negative. This does not change visibly when we include the subgrid diffusive flux divergence in the model as a part of "eddy flux divergence". We also computed κ for a "coarse-resolution mean state", obtained from averaging the model output in time and in $2^\circ \times 2^\circ$ blocks, and found qualitatively the same noisy results with both positive and negative signs. The negative values in κ implies that eddies are *not diffusing* the low-frequency isopycnal thickness gradient, but *tightening* the gradient, against the action of low-frequency flow advection that tends to weaken the gradient. This is, in fact, not surprising at all, considering that eddy activity is far from uniform and such spatial inhomogeneity in eddy activity is expected to result in eddy fluxes of temperature, density, etc, that are locally up the gradient of the background state (Plumb, 1979; Marshall and Shutts, 1981; Nakamura, 1998). Thus, κ field is expected to show both positive and negative values so long as the low-frequency (both in time and space) field resolves such inhomogeneity in eddy activity. Diagnoses of this model output by Nakamura and Chao (1999b) show that eddy fluxes of quasi-geostrophic potential vorticity are up the gradient of the mean in non-negligible portion of the domain considered. They also find that eddy fluxes of

density are up the gradient of the mean in many areas. Note that up-gradient eddy fluxes of isopycnal thickness have qualitatively the same effect as do up-gradient eddy momentum fluxes; they tend to sharpen a density front and accelerate the jet at the front.

One major assumption involved in the use of a positive constant value for κ , suggested by GM90 and GM95, is that eddy fluxes weaken the gradient of low-frequency isopycnal layer thickness. Where this assumption is valid, κ is expected to have a positive sign. Obviously, at least in the flows simulated by the eddy-resolving model presented here, this assumption is not valid about half of the time in the vicinity of the model GS. This possibility was, in fact, suggested by GM90. The parameterization scheme proposed by GM90 and GM95 with a positive constant for κ does not represent the processes occurring in the model and, probably, also in reality about half of the time; high-frequency eddies often tighten the gradient of low-frequency isopycnal thickness locally rather than diffusing it. A slightly different parameterization suggested by Treguier et al. (1997), based on an assumption of down-gradient eddy quasi-geostrophic potential vorticity fluxes, is likely to suffer from the same problem, since calculations of eddy quasi-geostrophic potential vorticity fluxes show a robust up-gradient character in many locations in the vicinity of the model GS (Nakamura and Chao, 1999b). The parameterization should yield eddy-induced isopycnal thickness fluxes that act against the fluxes by the low-frequency flow. In height coordinate models, the practical usefulness of the GM parameterization arises from its ability to represent the effect of the high-frequency eddy flux divergence that usually have a strong tendency to cancel the low-frequency flow flux divergence through the aforementioned representation of the total advection velocity in a form of the transformed Eulerian mean velocity. This aspect is in agreement with a simple time-mean balance consideration of an adiabatic-inviscid system in which all eddies are resolved, *viz*, $\nabla \cdot \overline{\mathbf{V}'\sigma'} = -\nabla \cdot (\overline{\mathbf{V}}\bar{\sigma})$. Negative κ is required when and where the resolved low-frequency flow tends to destroy the gradient in the low-frequency isopycnal thickness

in order to ensure this property. If only positive values are used for κ , a steady state obtained from a model integration with the GM parameterization is bound to suffer from unrealistic features. For example, let us consider a case in which a model is initialized with a steady state of a real ocean and integrated in time with the GM parameterization with positive values for κ . Clearly, at locations where eddies are tightening the low-frequency isopycnal thickness gradient in the real ocean, the model solution will drift toward an unrealistic steady state in which a balance among effects of the low-frequency flux divergence, parameterized eddy flux divergence, and diabatic processes on the low-frequency density field is achieved. Since the parameterized eddy flux divergence is forced to have a destructive effect on the low-frequency isopycnal thickness gradient in the new steady state, the low-frequency density field in the new steady state must have drifted to an unrealistic state so that an unrealistic balance among the three forcing factors can be established. A realistic steady state is obtained only if a κ field that establishes a realistic forcing balance is used.

From a visual inspection of κ time series, we found that κ shows large fluctuations in time, changing in both sign and magnitude, and that the maximum positive and negative values at a given location have very similar absolute values. In fact, positive and negative values at a given location tend to cancel out each other in the time mean to the extent such that simple time averages of κ show extremely small values in most of the domain with both positive and negative signs. The averages do not show any meaningful structure and, also, do not have the physical meaning of κ . Thus, we will show the results by plotting \log_{10} of the time-mean $|\kappa|$, calculated from all of the available time frames for the diagnosed κ , to show representative magnitudes of κ over the period considered. We will also show the ratio of time frames with positive κ to the total time frames. The time-mean $|\kappa|$ is denoted by $[|\kappa|]$. Fig 2 shows $\log_{10}[|\kappa|]$, calculated with a 150-day filter and averaged over the 300 time frames or 900 days, at selected levels. Time series of κ and $\log_{10}[|\kappa|]$ computed with a 360-day filter show practically the same horizontal and vertical structures and temporal characteristics,

but with magnitudes that are approximately 100 times greater than those calculated with a 150-day filter (not shown). The $\log_{10}[|\kappa|]$ calculated with a 360-day filter is also slightly noisier, most likely due to a significantly shorter period and fewer time frames to calculate the averages from. The noisiness in Fig 2 is most likely due to aliasing that arises from the small sample size, only 300 time frames or 900 days. We expect the field to be smoothed if significantly greater number of time frames and longer period are used to calculate the time mean. Given the limitation on the computational resources available to us, it is not feasible to increase the size of the data set significantly.

A somewhat anticipated feature in these figures is large $[|\kappa|]$ along the model GS in the top 400m and between 1000m and 2500m. The values along the GS in the top 400m are on the order of $1000m^2s^{-1}$ to $10000m^2s^{-1}$ and are 1 to 2 orders of magnitude greater than those in the surroundings depending on the depth. The model GS becomes split once it reaches $45^\circ N$, producing the main branch that flows northeastward and weaker branches flowing northward. These branches appear to be associated with most of broader and less coherent areas of large $[|\kappa|]$ to the north of $45^\circ N$. Comparable values are seen also in the top 400m in the subtropics, where fairly active eddies are seen in the model solutions. Relatively small values are seen to the east of the main branch of the model GS and north of $40^\circ N$ at most of the depths. Values in this relatively quiet region is about an order of magnitude smaller than those in more active regions. Also, relatively small values are seen in the Labrador Sea at most of the depths, again, except for a layer between 500m and 1000m. The horizontal structure of κ in the top 400m shows a strong resemblance to that of the Eady baroclinic wave growth rate calculated from the Levitus climatology by Treguier et al. (1997), suggesting that the magnitude of κ is proportional to the growth rate of unstable baroclinic waves in the Eady problem near the surface. The horizontal structure of $[|\kappa|]$ near the surface also shows a notable resemblance to that of observed sea surface height variance and eddy kinetic energy (e.g., Stammer et al.,

1996), although the $[\kappa]$ structure does not show the sharp northward turn toward the Northwest Corner in large values due to the model's deficiency in reproducing the northward turn in the GS. An interesting depth dependence of $[\kappa]$ is also evident in the results. Despite larger eddy fluxes and larger eddy kinetic and potential energies near the surface, $[\kappa]$ does not show the largest values near the surface. As a rule, $[\kappa]$ increases with depth and gradually loses horizontal structures at deeper levels. The larger values at depths arise from weak spatial variations in the low-frequency isopycnal slopes. We note, however, that it was necessary to assume that the spatial variations in κ are negligible compared to those in the low-frequency isopycnal slope in deriving the formula used to diagnose κ . Therefore, the formula used here may not resolve the spatial structure of κ very accurately. We also suspect that the profile of κ shown here is dependent on the vertical resolution of the model, which varies with depth, and its output used here to compute κ . We also find that $[\kappa]$ along the model GS is smaller than the surrounding between 400m and 800m or so.

The horizontal and vertical structures of $[\kappa]$ described above are also found in $[\kappa]$ calculated with a 360-day filter. However, values of $[\kappa]$ calculated with a 360-day filter are approximately 100 times greater than those computed with a 150-day filter. It suggests that values of $[\kappa]$ depend on how "a high-frequency eddy" is defined. When the model's subgrid diffusive flux divergence is included in $\nabla \cdot \overline{\mathbf{V}'\sigma'}$, the gross horizontal and vertical structures are unaffected, while values of $[\kappa]$ decrease by almost an order of magnitude in most of the domain. Since the model grid is not sufficiently high to resolve all high-frequency quasi-horizontal eddies, at least some of the model subgrid diffusive fluxes should be considered as a part of high-frequency eddy fluxes. The contribution of the subgrid diffusive flux divergence to the "total eddy flux divergence" is large near the surface where the gradients in $\bar{\sigma}$ are large. We note that the un-resolved part of the eddy flux divergence tends to counteract the divergence of the resolved part of the eddy fluxes, but does not change the characteristics of the $[\kappa]$ structure.

To examine the sense of the low-frequency isopycnal thickness gradient forcing by high-frequency eddies, we calculated the fractional ratio of the number of time frames of positive κ to the total time frames for which κ is calculated. Fig 3 shows the fractional ratio at 370m. To calculate the ratio, simply the total number of time frames with positive κ is counted for each grid point and divided by the total number of time frames for which κ is diagnosed. The top and bottom figures show, respectively, the ratio for calculations with a 150-day filter and a 360-day filter. Due to the larger sample size, 300 time frames as compared to 72 time frames, the ratio for the 150-day filter calculation is much less noisy than that for the 360-day filter calculation. The ratio for the 150-day filter calculation is close to 0.5 in most of the domain, whereas the ratio for the 360-day filter calculation shows a great spatial variations ranging from almost 0 to almost 1. These characteristics are seen at all levels and do not change visibly when the model's subgrid diffusive flux divergence is included in the calculation of κ . During the period of 900 days, for which κ is computed with a 150-day filter, the high-frequency eddies act to tighten the gradient in the low-frequency isopycnal thickness about half of the time in most of the domain. We speculate that the ratio for the 360-day filter calculation would appear much like that for the 150-day filter calculation if substantially longer period and more time frames are used to calculate the ratio.

A very intriguing aspect of this ratio is that the basin average at each level is very close to 0.50 for both the 150-day filter calculation and the 360-day filter calculation, despite the great difference in the noisiness in the horizontal structure of the ratio. The range of the ratio for the 150-day filter calculation averaged at each level is from 0.492 to 0.509, with the average for the entire 3-dimensional domain being 0.503. The range of the ratio for the 360-day filter calculation averaged at each level is from 0.488 to 0.509, with the average for the entire 3-dimensional domain being 0.498. Furthermore, when the subgrid diffusive flux divergence is included in the 150-day filter calculation, the ratio averaged at each level shows an almost-

monotonic decrease from 0.555 near the surface to 0.507 at 1375m, then very close to 0.500 farther below. The average for the entire 3-dimensional domain is 0.520 with the diffusive flux divergence. We speculate that forcing of the low-frequency density structure is accomplished primarily by the resolved high-frequency eddies that transfer the surface diabatic forcing into high-frequency eddy available potential energy and then into low-frequency available potential energy, in the eddy-resolving model used here. We interpret the average ratio of 0.50 as an indication of a nonlinear balance between the resolved high-frequency and low-frequency flows in the model; high-frequency eddies force the low-frequency state until it reaches a certain point at which the low-frequency state starts releasing the available potential energy to high-frequency eddies. However, we also speculate that high-frequency eddies and smaller-scale motions generated by nonlinear behaviors of these eddies in the real ocean are a net sink of the low-frequency available potential energy on the basin-scale, particularly in the upper part of the ocean, say, the top 1000m or so. This speculation is based on the clear signature of the net effect of the eddy flux divergence that tends to destroy the low-frequency isopycnal thickness gradient in the upper 1000m of the model when the model's subgrid diffusive flux divergence is included as a part of the total eddy flux divergence in calculating κ (horizontal averages of the ratio of positive κ are consistently greater than 0.5 in the top 1000m and decrease from the surface). The model resolution is not sufficiently high to capture eddy fluxes associated with filaments that are generated by eddies and is represented by the model's subgrid diffusive fluxes. Therefore, one may argue that the net basin-averaged value of κ is indeed positive, assuming that the magnitude of negative κ is the same as that of positive κ .

5 Concluding remarks

The results reported here strongly suggest that κ used in coarse-resolution model integrations needs to be diagnosed from the large-scale density structure resolved

by the models. Appropriately diagnosed variable κ is likely to mimic the fact that eddy tracer flux divergence tends to cancel the mean flow flux divergence better than a constant κ . Approaches suggested by Visbeck et al. (1997) and Treguier et al. (1997) may provide such diagnosed κ for some improvements in simulations of large-scale oceanic states by coarse-resolution models. We have not computed κ for a different formulation of eddy-induced velocity suggested by Treguier et al. (1997), since the focus here is κ for the GM scheme. However, from their Eq 37 and what we observe in our diagnoses of quasi-geostrophic potential vorticity fields and eddy fluxes (Nakamura and Chao, 1999a, 1999b), we suspect that horizontal structures of κ for the parameterization suggested by Treguier et al. (1997) may look similar to those presented here.

Unpublished calculations by Nakamura and Marshall have demonstrated that simulation of temperature and salinity in a coarse-resolution ocean GCM can be improved further by the use of spatially and temporally varying κ in a form suggested by Visbeck et al. (1997). However, they still note substantial deviations of the model state from the observed state. At least a part of the reason for this problem is that the diagnosed κ used by Nakamura and Marshall does not allow for negative κ required when and where the resolved low-frequency flow tends to destroy the isopycnal thickness gradient. Diagnosing a κ field, at each time step, that appropriately represents the tendency of eddy flux divergence to oppose the low-frequency flux divergence and still allows realistic evolution of the low-frequency density field is at least extremely challenging, if not impossible. If such a diagnostic procedure for κ is developed, however, it is likely to improve ocean simulation by coarse-resolution ocean circulation models when applied appropriately with the GM parameterization. Finally, we note that the values of κ shown here may not be very close to the true values that would be obtained from diagnoses of real oceanic data. The model underestimates both the mean and eddy kinetic energies and is likely to have underestimated generation of eddy potential energy and its conversion into the mean potential energy. Also, the

horizontal and vertical resolutions may not be sufficient to calculate the derivatives of low-frequency isopycnal slopes. We also made one simplifying assumption of slowly-varying κ with respect to low-frequency isopycnal slopes to obtain the diagnostic formula for κ . We suggest that more realistic values of κ should be obtained from diagnoses that do not suffer from these uncertainty factors. We emphasize, however, that the values of κ depend strongly on the time scale used to define the eddy and the low-frequency state and, thus, that one should not apply any diagnosed values to coarse-resolution ocean model integrations blindly.

Acknowledgement

The research described in this paper was carried out by the Jet Propulsion Laboratory (JPL), California Institute of Technology, under contract with National Aeronautics and Space Administration. Computations were carried out on the 256-processor Cray T3D through the JPL Supercomputing Project. Nakamura is indebted to John Marshall for stimulating conversations that led to this series of diagnoses. We are grateful to Jim McWilliams for suggesting the calculations shown in Fig 3. We also wish to thank Vittorio Canuto for helpful comments on the original version of the manuscript.

References

- Andrews, D., and M. McIntyre, 1976: Planetary waves in horizontal and vertical shear: The generalized Eliassen-Palm relation and the mean zonal acceleration. *J. Atmos. Sci.*, **33**, 2031-2048.
- Beckman, A., C.W. Böning, C. Köberle, and J. Willebrand, 1994: Effects of increased horizontal resolution in a simulation of the North Atlantic Ocean. *J. Phys. Oceanogr.*, **24**, 326-344.
- Bryan, F.O., and W.R. Holland, 1989: A high resolution simulation of the wind- and thermohaline-driven circulation in the North Atlantic Ocean. *'Aha Huliko'a Parameterization of Small-Scale Processes*, P. Muller and D. Henderson, Eds., Hawaii Institute of Geophysics, 99-115.
- Chao, Y., A. Gangopadhyay, F.O. Bryan, and W.R. Holland, 1996: Modeling the Gulf Stream: How far from reality? *Geophys. Res. Lett.*, **23**, 3155-3158.
- Danabasoglu, G., J.C. McWilliams, and P.R. Gent, 1994: The role of mesoscale tracer transports in the global ocean circulation. *Science*, **264**, 1123-1126.
- Duffy, P.B., P. Eltgroth, A.J. Bourgeois, and K. Caldeira, 1995a: Effect of improved subgrid scale transport of tracers on uptake of bomb radiocarbon in the GFDL ocean general circulation model. *Geophys. Res. Lett.*, **22**, 1065-1068.
- Duffy, P.B., D. Eliason, A.J. Bourgeois, and C. Covey, 1995b: Simulation of bomb radiocarbon in two ocean general circulation models. *J. Geophys. Res.*, **100**, 22545-22565.
- Duffy, P.B., K. Caldeira, J. Selvaggi, and M.I. Hoffert, 1997: Effects of subgrid-scale mixing parameterizations on simulated distributions of natural ^{14}C , temperature, and salinity in a three-dimensional ocean general circulation model. *J. Phys. Oceanogr.*, **27**, 498-523.
- Eady, E.T., 1949: Long waves and cyclone waves. *Tellus*, **1**, 33-52.
- Gent, P.R. and J.C. McWilliams, 1990: Isopycnal mixing in ocean circulation models.

- J. Phys. Oceanogr.*, **20**, 150-155.
- Gent, P.R., J. Willebrand, T.J. McDougall, and J.C. McWilliams, 1995: Parameterizing eddy-induced tracer transports in ocean circulation models. *J. Phys. Oceanogr.*, **25**, 463-474.
- Green, J.S., 1970: Transfer properties of the large-scale eddies and the general circulation of the atmosphere. *Quart. J. Roy. Meteor. Soc.*, **96**, 157-185.
- Held, I.M. and V.D. Larichev, 1996: A scaling theory for horizontally homogeneous, baroclinically unstable flow on a beta plane. *J. Atmos. Sci.*, **53**, 946-952.
- Lau, N.-C. and K.M. Lau, 1984: The structure and energetics of midlatitude disturbances accompanying cold air outbreaks over East Asia. *Mon. Wea. Rev.*, **112**, 1309-1327.
- Levitus, S., 1982: *Climatological Atlas of the World Ocean.*, NOAA Prof. Paper 13. U.S. Govt. Printing Office, Whashington, D.C., 173pp.
- Levitus, S., 1994: World Ocean Atlas 1994 CD-Rom Sets. *National Oceanographic Data Center Informal Report*, **13**.
- Marshall, J.C. and G. Shutts, 1981: A note on rotational and divergent eddy fluxes. *J. Phys. Oceanogr.*, **11**, 1677-1680.
- Nakamura, M., 1998: On modified rotational and divergent eddy fluxes and their application to blocking diagnoses. *Quart. J. Roy. Meteor.*, **124**, 341-352.
- Nakamura, M., and Y. Chao, 1999a: Diagnoses of an eddy-resolving Atlantic Ocean model simulation in the vicinity of the Gulf Stream. Part I: Potential vorticity. Submitted to *J. Phys. Oceanogr.*
- Nakamura, M., and Y. Chao, 1999b: Diagnoses of an eddy-resolving Atlantic Ocean model simulation in the vicinity of the Gulf Stream. Part II: Eddy potential enstrophy and eddy potential vorticity fluxes. Submitted to *J. Phys. Oceanogr.*
- Owens, W.B., 1991: A statistical description of the mean circulation and eddy variability in the northwestern Atlantic using SOFAR floats. *Prog. Oceanog.*, **28**, 257-303.

- Plumb, R.A., 1979: Eddy fluxes of conserved quantities by small-amplitude waves. *J. Atmos. Sci.*, **36**, 1699-1704.
- Redi, M., 1982: Oceanic isopycnal mixing by coordinate rotation. *J. Phys. Oceanogr.*, **12**, 1154-1157.
- Rix, N.H. and J. Willebrand, 1996: Parameterization of mesoscale eddies as inferred from a high-resolution circulation model. *J. Phys. Oceanogr.*, **26**, 2281-2285.
- Richardson, P.L., 1993: A census of eddies observed in North Atlantic SOFAR float data. *Prog. Oceanog.*, **31**, 1-50.
- Robitaille, C.Y., and A.J. Weaver, 1995: Validation of sub-gridscale mixing schemes using CFCs in a global ocean model. *Geophys. Res. Lett.*, **22**, 2917-2920.
- Schmitz, W.J.Jr., 1996: *On the World Ocean Circulation: Volume I: Some Global Features/North Atlantic Circulation*. Woods Hole Oceanographic Institution Technical Report, WHOI-96-03, pp141.
- Semtner, A.J., and R.M. Chervin, 1992: Ocean general circulation from a global eddy-resolving model. *J. Geophys. Res.*, **97**, 5493-5550.
- Smith, R.D., J.K. Dukowicz, and R.C. Malone, 1992: Parallel ocean general circulation modeling. *Physica D*, **60**, 38-61.
- Solomon, H., 1971: On the representation of isentropic mixing in ocean circulation models. *J. Phys. Oceanogr.*, **1**, 233-234.
- Stammer, D, R. Tokmakian, A. Semtner, and C. Wunsch, 1996: How well does a 1/4 degrees global circulation model simulate large-scale oceanic observations? *J. Geophys. Res.*, **101**, 25779-25811.
- Stone, P.H., 1972: A simplified radiative-dynamical model for the static stability of rotating atmospheres. *J. Atmos. Sci.*, **29**, 405-418.
- Treguier, A.M., I.M. Held, and V.D. Larichev, 1997: Parameterization of quasi-geostrophic eddies in primitive equation ocean models. *J. Phys. Oceanogr.*, **27**, 567-580.

Visbeck, M., J.C. Marshall, T. Haine, M.A. Spall, 1997: Specification of eddy transfer coefficients in coarse-resolution ocean circulation models. *J. Phys. Oceanogr.*, **27**, 381-402.

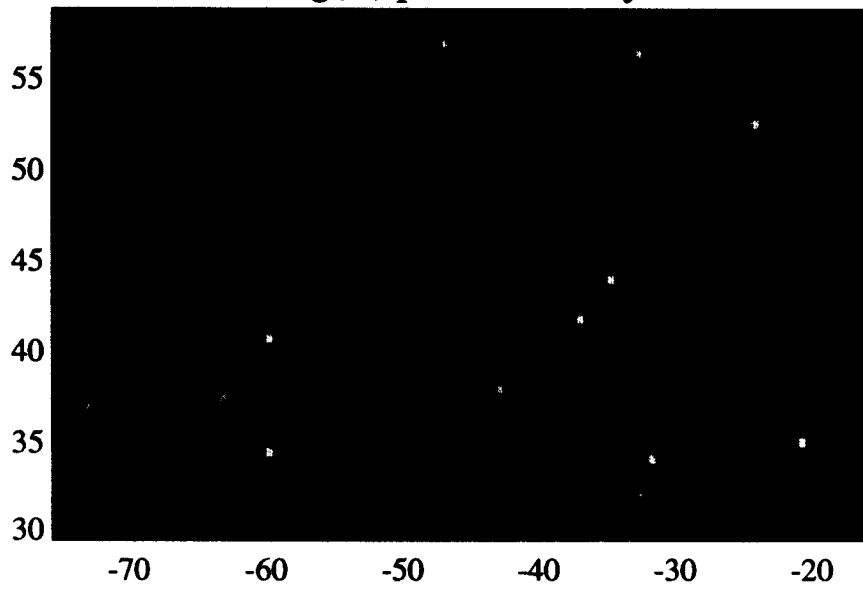
Figure Captions

Figure 1. A snapshot of κ at 370m. Top panel shows $\log_{10}(\kappa)$ for positive values of κ only, while the bottom panel shows $\log_{10}(-\kappa)$ for negative values of κ only. Areas where values are missing are shaded black. Gray is used to indicate areas of negative and positive values, respectively, in the top and bottom panels. Units of κ are m^2s^{-1} .

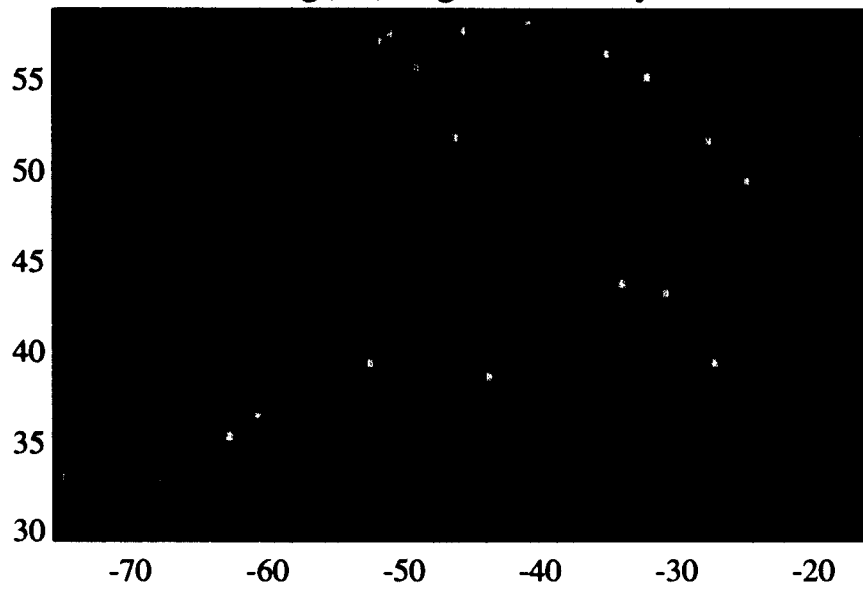
Figure 2. Time average of absolute values of κ at (a) 140m, (b) 577m, and (c) 1875m. The plotted values are \log_{10} of the time average. Units of κ are m^2s^{-1} .

Figure 3. Fractional ratio of the number of time frames with positive κ to the total time frames for which κ is calculated. The top and the bottom, respectively, show the ratio for the calculations made with a 150-day filter and a 360-day filter at 370m.

log(K) positive K only

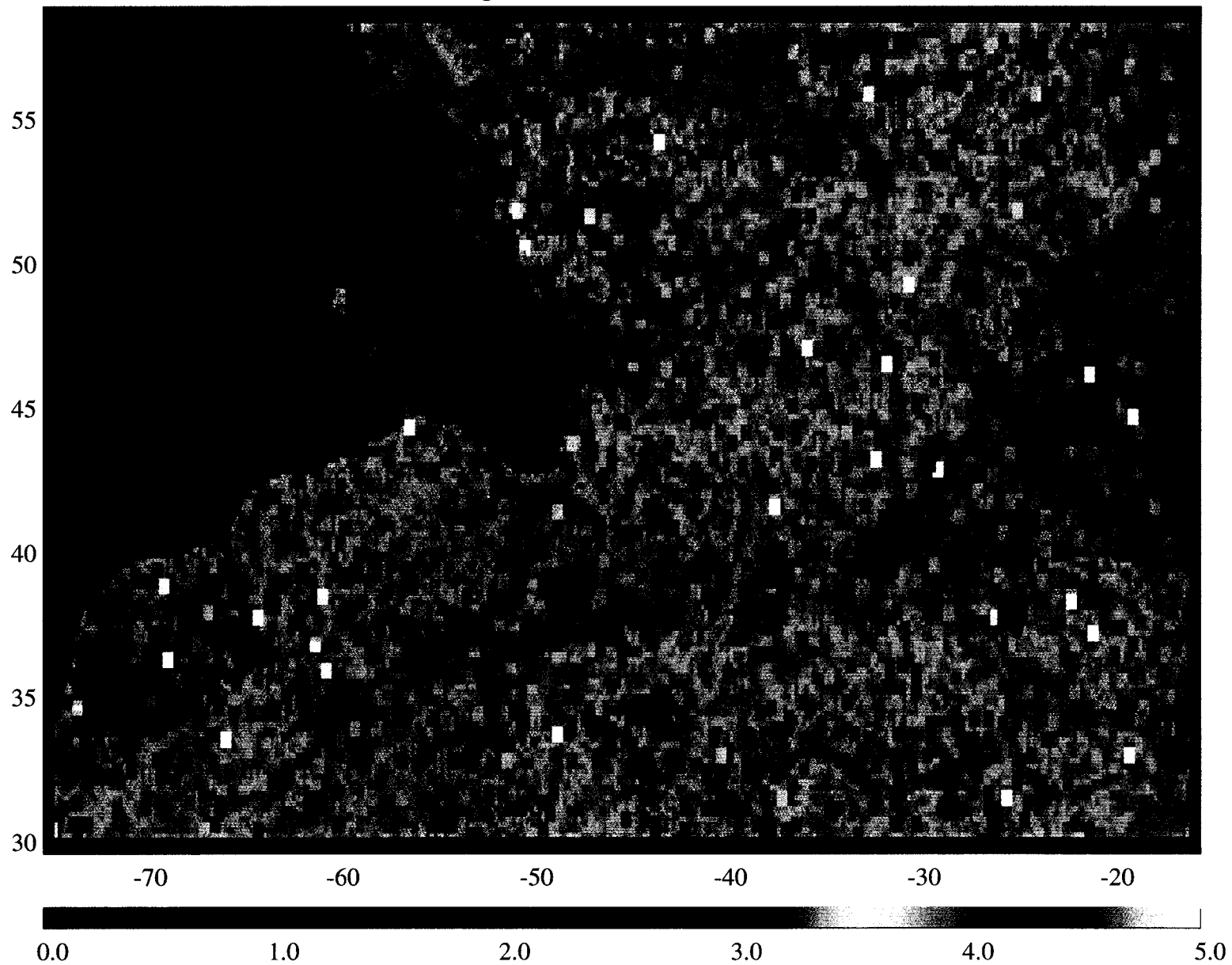


log(-K) negative K only



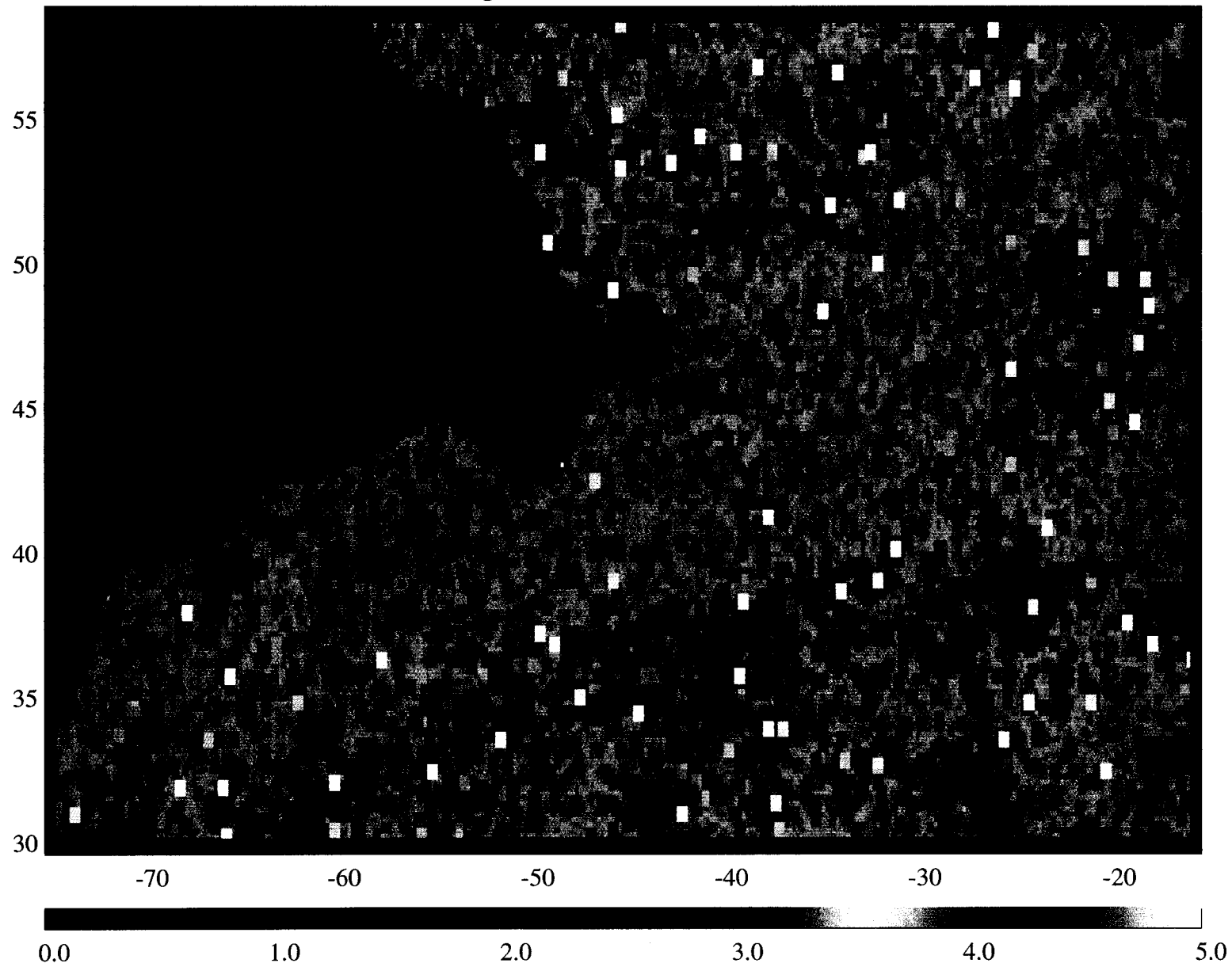
/

$\log_{10}(\text{mean } |K_h|) \text{ at } 140\text{m}$



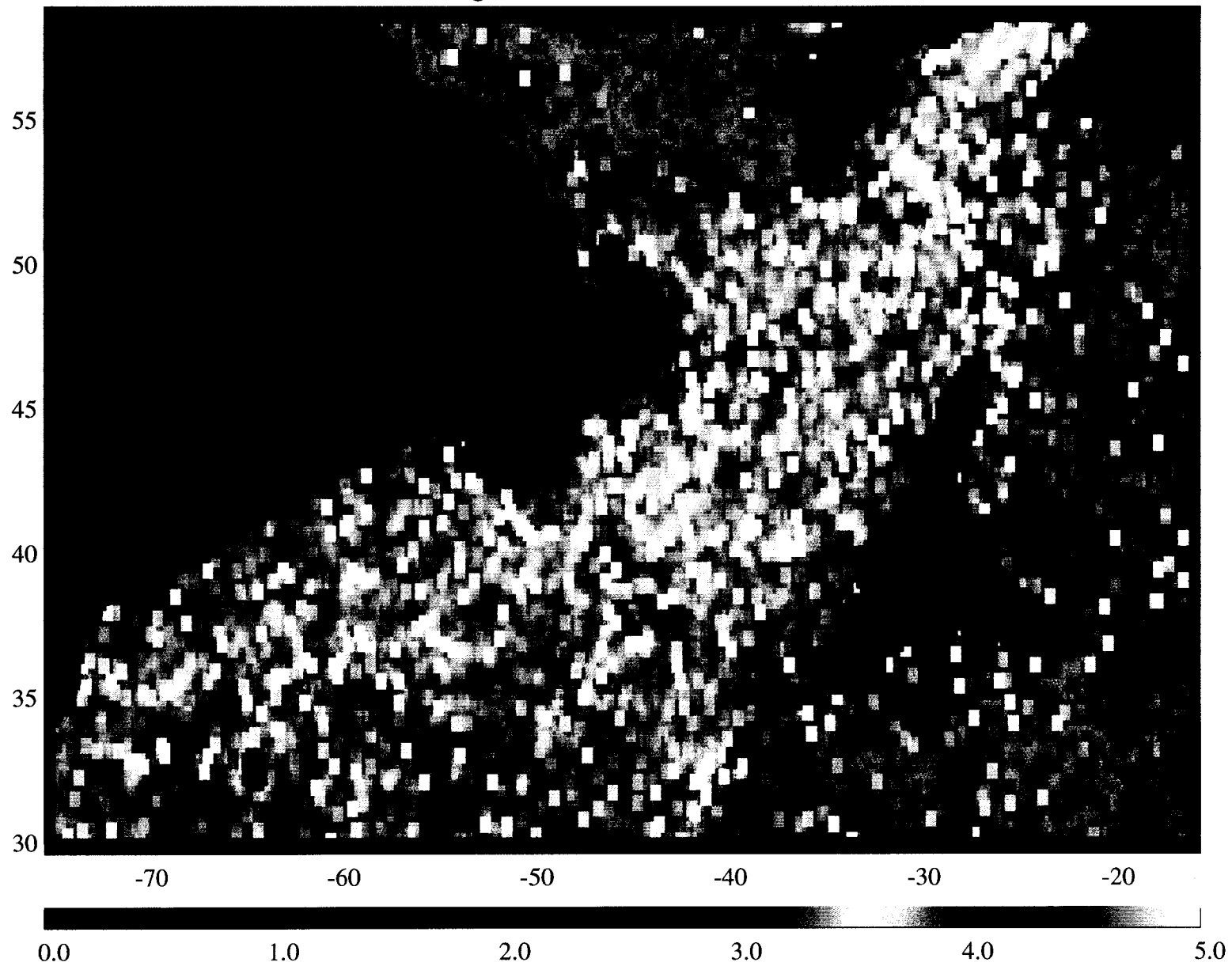
2a

$\log_{10}(\text{mean } |Kh|) \text{ at } 577\text{m}$



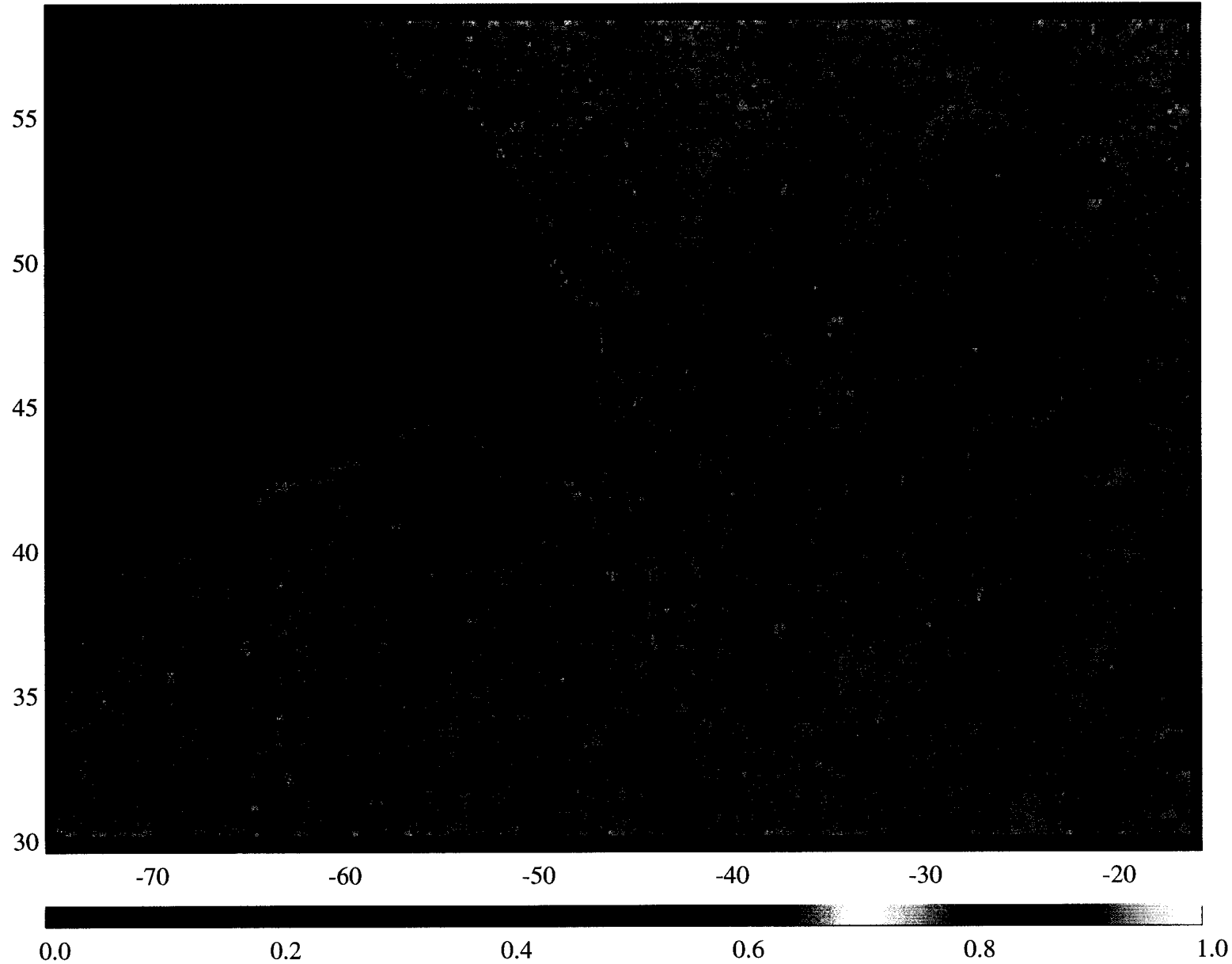
2b

$\log_{10}(\text{mean } |Kh|) \text{ at } 1875\text{m}$



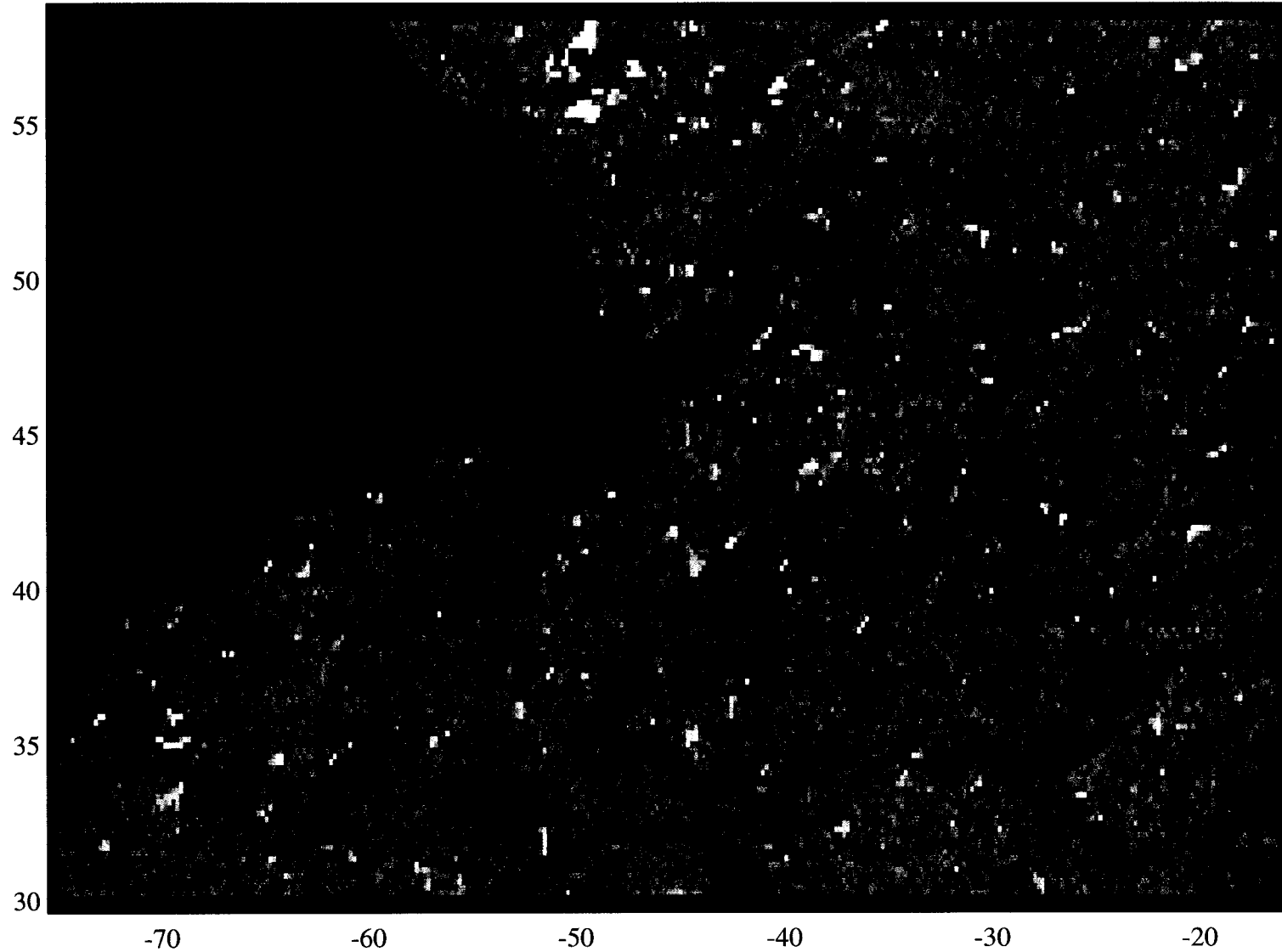
2c

Ratio of positive Kh at 370m



3top

Ratio of positive Kh at 370m



3 btm